Multistage osmotically assisted reverse osmosis process for concentrating solutions using hollow fiber membrane modules

Nakagawa, Keizo ; Togo, Norihiro ; Takagi, Ryosuke ; Shintani, Takuji ; Yoshioka, Tomohisa ; Kamio, Eiji ; Matsuyama, Hideto

(Citation)
Chemical Engineering Research and Design,162:117-124

(Issue Date)
2020-10

(Resource Type)
journal article

(Version)
Accepted Manuscript

(URL)
https://hdl.handle.net/20.500.14094/90008083

Multistage osmotically assisted reverse osmosis process for concentrating solutions using hollow fiber membrane modules

Keizo Nakagawa[1, 3]*, Norihiro Togo[1], Ryosuke Takagi[2, 3], Takuji Shintani[1, 3], Tomohisa Yoshioka[1, 3], Eiji Kamio[2, 3], Hideto Matsuyama[1, 2, 3]*

[1]*Graduate School of Science, Technology, and Innovation, Kobe University, 1-1 Rokkodai, Nada, Kobe 657-8501, Japan*

[2]*Department of Chemical Science and Engineering, Kobe University, 1-1 Rokkodai, Nada, Kobe 657-8501, Japan*

[3]*Reserach Center for Membrane and Film Technology, Kobe University, 1-1 Rokkodai, Nada, Kobe 657-8501, Japan*

*Corresponding Authors:

E-mail addresses: k.nakagawa@port.kobe-u.ac.jp (K. Nakagawa), matuyama@kobe-u.ac.jp (H. Matsuyama)

Abstract

Reverse osmosis (RO) is commonly used to concentrate solutions in food preparation and environmental applications among others. Limitations on the applied pressure, which must be higher than the osmotic pressure of the feed solution, determine the concentration that can be achieved by RO. Recently, an osmotically assisted reverse osmosis (OARO) system that can be operated even with low applied pressure has been suggested as a new concentration process. In this study, we performed concentration tests on a multistage OARO system that used two types of hollow fiber (HF) membrane modules made from cellulose triacetate with different numbers of HFs. Water permeated through the membrane and the concentration increased as it progressed through the modules, even when using concentrated NaCl solutions (1.0 and 2.0 M) with low applied pressures (10 and 15 bar). The concentration increased in each of ten stages in a multistage concentration test. Water flux and concentration ratio were strongly influenced by the internal concentration polarization in the modules.

Keywords: osmotically assisted reverse osmosis; multistage concentration process; hollow fiber membrane module; cellulose triacetate membrane; concentration polarization

1. Introduction

The concentration of solutions is a very important process in wastewater treatment and industrial applications. In the food industry, especially for juice production (Alvarez et al., 1997; Jesus et al., 2007; Jiao et al., 2004; Petrotos and Lazarides, 2001), solution concentration is used to decrease the volume of product to increase shelf-life and decrease transportation costs. The concentration processes used in the food industry are evaporation, vacuum concentration, freeze concentration, and membrane separation (Alvarez et al., 1997; Jiao et al., 2004). Membrane processes are widely used to concentrate juices because of their low operating temperatures and low energy consumption. Juice must be concentrated at low temperature to avoid thermal damage to the product (Alvarez et al., 1997; Jesus et al., 2007; Jiao et al., 2004; Petrotos and Lazarides, 2001). Reverse osmosis (RO) is usually employed (Alvarez et al., 1997; Jesus et al., 2007; Jiao et al., 2004; Petrotos and Lazarides, 2001) for this purpose, but the concentrations achievable are limited because RO requires that the applied pressure be higher than the osmotic pressure of the feed solution (Jiao et al., 2004; Petrotos and Lazarides, 2001). Forward osmosis (FO) (Chekli et al., 2016; Sant'Anna et al., 2012; Shibuya et al., 2017; Zhang et al., 2018) is another option, but further development of draw solutions is required to make this process viable (Ge et al., 2013).

Recently, osmotically assisted reverse osmosis (OARO) has been suggested as an alternative to normal RO (Bartholomew et al., 2018, 2017; Chen and Yip, 2018; Kim et al., 2018a, 2018b; Park et al., 2017; Togo et al., 2019). As shown in Fig. 1, in OARO, the same solutions with the same osmotic pressure are supplied to both sides of the RO membrane. Water permeates through the membrane as a result of applying pressure that does not depend on the feed concentration because there is no osmotic pressure difference across the membrane. Laboratory-scale systems have been tested and theoretical estimates of the energy consumption of the process have been published. Bartholomew et al. proposed a desalination process utilizing OARO (Bartholomew et al., 2018, 2017). By comparing the OARO with evaporation and RO systems, they demonstrated that the water recovery rate of the OARO process was higher than that of RO, and the energy consumption of the process was lower than that of the evaporation system because no energy was expended to heat the feed. Our previous work describes a concentration test on NaCl solution and theoretical calculations for an OARO system using a pilot-scale hollow fiber (HF) membrane module (Togo et al., 2019). The concentration gradient and internal concentration polarization (ICP) (Fig.2) in the module affected the water flux and the degree of concentration.

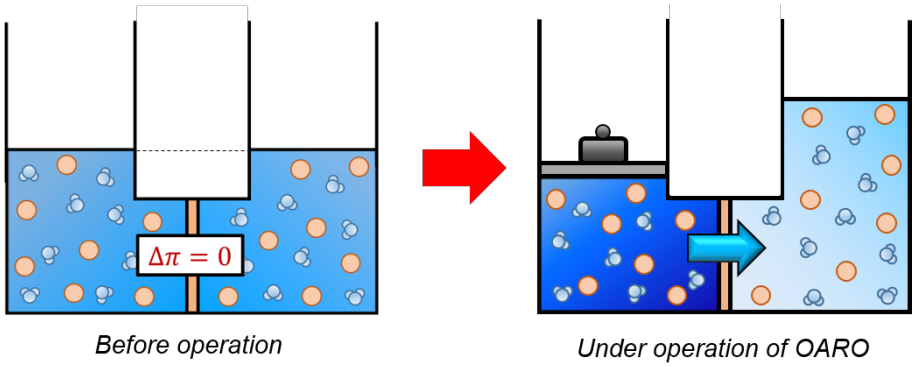

Fig. 1 Concept of osmotically assisted reverse osmosis (OARO).

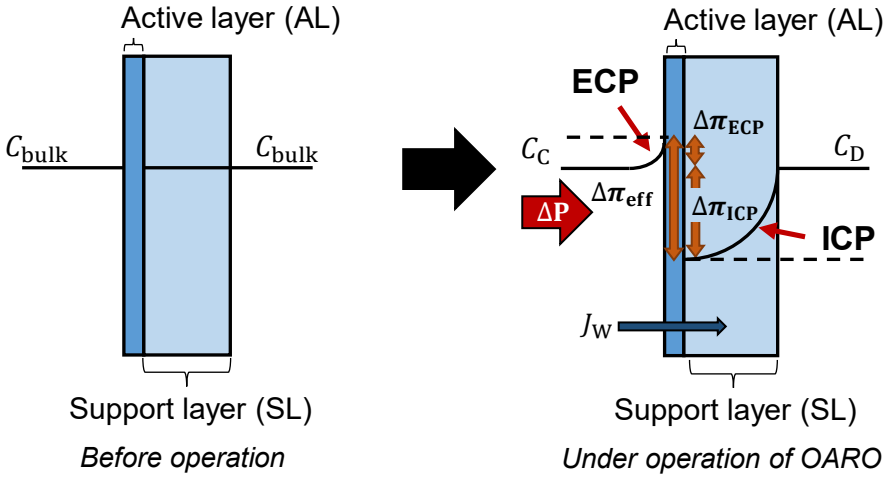

Fig. 2 Concentration polarization under OARO operation. ECP: external concentration polarization, ICP: internal concentration polarization, $\Delta\pi_{eff}$: effective osmotic pressure difference at interface.

The degree of concentration achievable using the OARO process is still too low even though the OARO process performs better than RO in this regard. A multistage process is one solution to this problem, but multistage OARO processes have so far only been studied theoretically and not, to the best of our knowledge, experimentally (Bartholomew et al., 2018, 2017; Chen and Yip, 2018). In this

paper, solution concentration using multistage OARO system was studied experimentally, and the effects of initial feed concentration and applied pressure were investigated.

2. Material and methods

2.1. Materials and membrane module

Aqueous NaCl (99.5%, FUJIFILM Wako Pure Chemical Corporation, Osaka, Japan) solution was used as a model feed solution. The HF membrane module provided by Toyobo (Osaka, Japan) was used as a membrane module. Figure 3 shows a schematic of the module. The HF membranes with the active layer on the shell side were made from cellulose triacetate (CTA) and were arranged in parallel within a cylindrical housing. The CTA HF membrane can be used under the applied pressure of less than around 20 bar. The HF membrane module used in this research contains either 90 or 180 HFs. The detailed specifications of the HF modules are shown in Table 1. The modules with 90 HFs and 180 HFs are designated as HF90 and HF180, respectively.

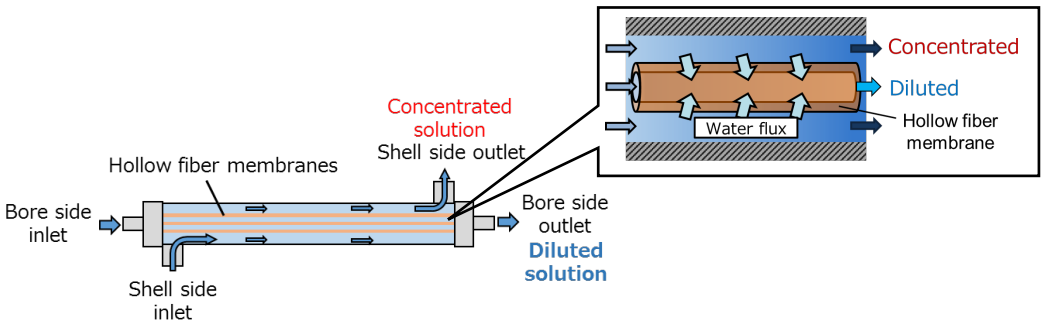

Fig. 3 Schematic of HF membrane module.

Table 1 Specifications of HF membrane modules

Number of HF [-]	HF inner diameter [μm]	HF outer diameter [μm]	Effective length [m]	Effective membrane area [m^2]	Water permeability coefficient [LMH/bar]	Salt permeability coefficient [LMH]
90	105	202	0.245	1.40×10^{-2}	0.347	4.59×10^{-3}
180	105	202	0.245	2.80×10^{-2}	0.351	5.95×10^{-3}

2.2 Evaluation of membrane module

Figure 4 shows the equipment used to evaluate the module performance. One side of the HF membrane was closed and the other side was left open. Pure water from a Milli-Q water system (Merck Millipore, Darmstadt, Germany) was supplied to the shell side of the HF at a flow rate of 75 mL/min, and a pressure of 2–15 bar was applied to the shell side. The mass of the water that permeated from the shell side into the bore side was measured every minute. The pure water flux, J_W (L m^{-2} h^{-1} (LMH)) was calculated using Eq. (1).

$$J_w = \frac{\Delta m}{A_m \times \Delta t \times \rho} \quad (1)$$

Here, Δm (g) indicates the weight of permeated water, A_m (m^2), the effective membrane area, Δt (h), the time, and ρ (g/L), the density of the permeated water. In this paper, ρ was assumed to be 1000 g/L. The water permeability coefficient of the membrane, A (LMH/bar) was calculated from Eq. (2).

$$A = \frac{J_W}{\Delta P} \quad (2)$$

Here, ΔP (bar) is the applied pressure.

To test salt rejection, 2000 ppm NaCl aqueous solution was supplied to shell side of the HF membrane at a flow rate of 75 mL/min, and a pressure of 5–15 bar was applied to the shell side. The salt rejection, R, was calculated using Eq. (3),

$$R = 1 - \frac{C_\mathrm{p}}{C_\mathrm{f}} \quad (3)$$

where C_p (mol/L) and C_f (mol/L) are the salt concentrations of the permeate and the feed, respectively. The salt concentration was determined from the electric conductivity of the solution as measured by a conductivity meter (ES-71, ES-33B, Horiba, Kyoto, Japan). The salt rejection is related to the salt permeability coefficient of the membrane, B (LMH), by Eq. (4) (McCutcheon and Elimelech, 2006; Yasukawa et al., 2015):

$$B = J_{W(NaCl)} \left(\frac{1-R}{R}\right) \exp\left(-\frac{J_{W(NaCl)}}{k_f}\right) \quad (4)$$

where $J_{W(NaCl)}$ indicates the water flux of NaCl aqueous solution. The mass transfer coefficient k_f (LMH) is given by Eq. (5) (McCutcheon and Elimelech, 2006; Yasukawa et al., 2015):

$$k_f = \frac{J_{W(NaCl)}}{\ln\left(\frac{\Delta P}{\pi_f - \pi_p}\left(1 - \frac{J_{W(NaCl)}}{J_W}\right)\right)} \quad (5)$$

where π_f and π_p are the osmotic pressures of the bulk feed solution and the permeate solution, respectively.

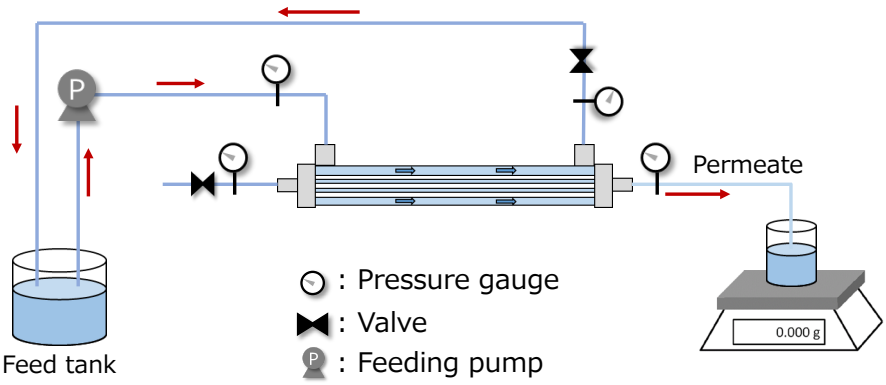

Fig. 4 Schematic of module evaluation system.

2.3 Feed solution concentration test

2.3.1 Single-stage concentration test

The H180 module is expected to have a higher concentration speed than the H90 module under the same applied pressure because the H180 membrane area is larger. On the other hand, the difference of the number of HFs in the modules will affect the water flux. The optimal packing densities for the

H90 and H180 modules were determined from single stage concentration tests and then used in the multistage concentration process.

Figure 5 shows a schematic of the single stage concentration process. The same feed solution was supplied to the shell and bore sides. The concentrated solution was returned to the feed tank and recirculated through the module. The concentration of the feed solution was determined by measuring its electric conductivity with a conductivity meter, EC-33B (Horiba, Ltd, Kyoto, Japan). The initial feed solution was 1.0 M NaCl, and the volume was 2.5 L. The feed solution was supplied to the shell side at a flow rate of 20 mL/min using a NP-KX-500P plunger pump (Nihon Seimitsu Kagaku Co. Ltd, Tokyo, Japan), and to the bore side at a flow rate of 5 mL/min using an NPL-120 plunger pump (Nihon Seimitsu Kagaku Co. Ltd). The linear velocities on the membrane surfaces were estimated to be 0.008 for H90 module and 0.009 m/s for H180 module. In addition, the initial linear velocities on the bore side were estimated to 0.107 m/s for H90 module and 0.053 m/s for H180 module. The bore-side flow rate was set as low as possible in order to reduce the pressure drop and enhance the water flux. The pressure difference across the membrane was kept at 15 bar, and the concentration test was performed for 180 minutes. The result for H90 module was compared with that for H180 module.

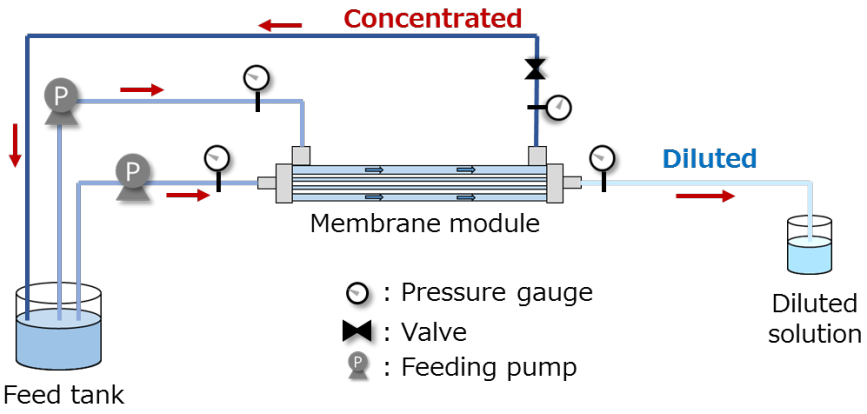

Fig. 5 Schematic of single stage concentration process.

2.3.2 Multistage concentration test

Figure 6 shows a schematic of two connected stages in the multistage concentration process. Two H180 modules were connected in series. The concentrate from the second module was supplied as the feed solution to the first module. By repeating this procedure, we experimentally performed a multistage OARO system with up to 10 stages.

Solutions of 1.0 M or 2.0 M NaCl in batches of 2.5 L were used as the initial feed solution, and 10 or 15 bars of external pressure were applied to the shell side of the module. The NaCl solution was initially supplied to the shell side of the first module at a flow rate of 50 ml/min and to the bore side at 2 ml/min. The shell-side solution was then concentrated, and the bore-side solution, diluted. The bore-side flow rate was maintained at 2 ml/min in all stages. The outlet from one module (concentration, flow rate, pressure) was fed to the inlet of the next stage. For example, the product of

the second stage was the input to the third stage. The shell -side flow rate decreased slightly at each stage. The applied pressure was the same in all stages.

The water flux at each stage was obtained by substituting Eq. (6) into Eq. (1).

$$\Delta m = Q_{bore.out} - Q_{bore,in} \quad (6)$$

Here, $Q_{bore.out}$ and $Q_{bore,in}$ indicate the weight of water (g) flow through the bore outlet and the inlet, respectively.

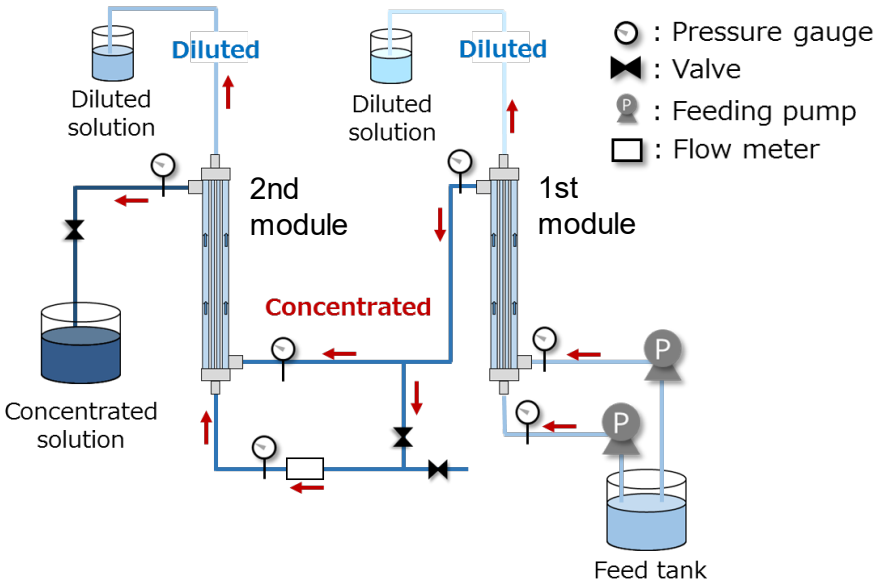

Fig. 6 Schematic of two connected stages in a multistage OARO process.

3. Results and discussion

3.1 Evaluation of membrane module

The flux of pure Milli-Q water flux was first measured. Figure 7 shows the water flux and salt permeability coefficient of each module as a function of applied pressure. The water flux increased

linearly with the applied pressure for both HF modules. The pure water permeability coefficients calculated from the gradient of water fluxes were 0.347 and 0.351 LMH/bar for the H90 and H180 modules, respectively. These data are included in Table 1. Figure 7(c) and (d) shows the salt permeability coefficient and the salt rejection of the H90 and H180 modules as a function of applied pressure. The salt permeability coefficient and the rejection were not significantly influenced by the applied pressure. The salt permeability coefficients were 4.59×10^{-3} and 5.95×10^{-3} LMH for the H90 and H180 modules, respectively (Table 1), which are very low values compared with other membranes (0.07–0.35 LMH) (Sukitpaneenit and Chung, 2012; Yasukawa et al., 2015; Zhang et al., 2010). These low salt permeability coefficients are reflected in the salt rejection performance of the modules, which both rejected over 99.6% of the salt in the feed solution.

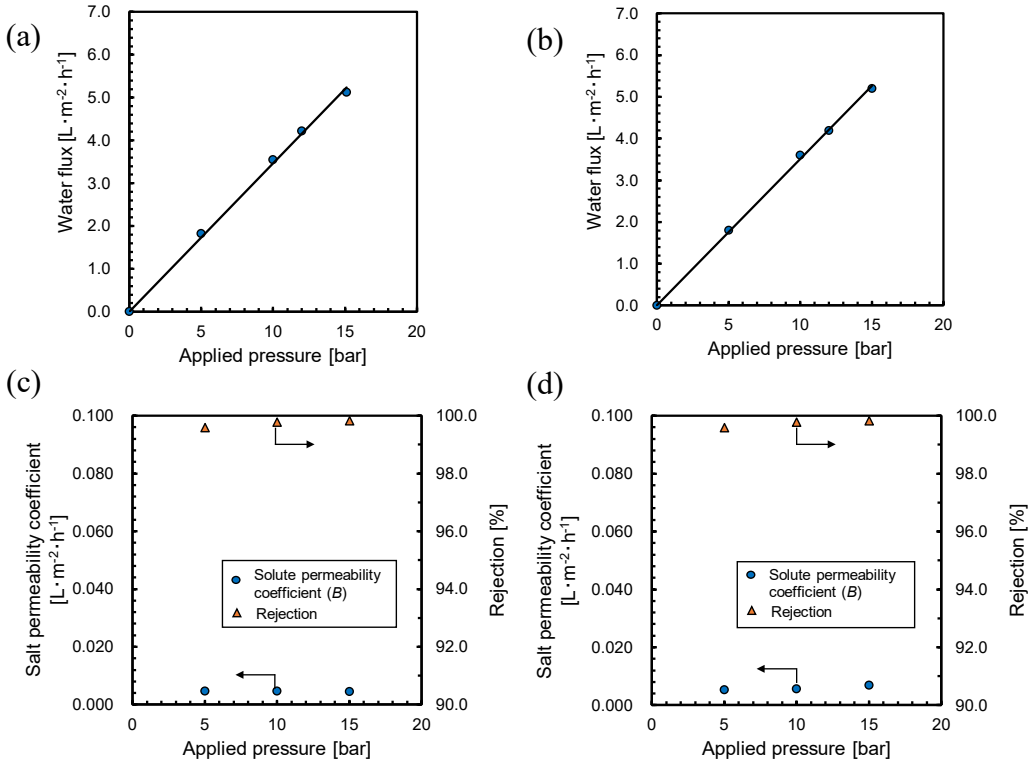

Fig. 7 Water flux (a, b) and salt permeability coefficient and rejection (c, d) of H90 (a, c) and H180 module (b, d) as a function of applied pressure.

3.2 Concentration tests

3.2.1 Single-stage concentration test

Single-stage concentration tests were performed on the H90 and H180 modules to determine which module was better for a multistage concentration process. In this experiment, 2.5 L of 1.0 M NaCl aqueous solution was used as the initial feed solution. Figure 8 shows the concentration of the shell-side solution and the water flux through the membrane as a function of operating time under an applied pressure of 15 bar. Water permeated through the membrane and the shell side solution grew

progressively more concentrated in both H90 and H180 modules, even with a feed NaCl solution concentration as high as 1.0 M NaCl (1.67 times the concentration in sea water) and at applied pressures as low as 15 bar.

The water flux was constant and did not depend on the operating time in both H90 and H180 modules, demonstrating that the effect of salt concentration on water flux was not time-dependent under these operating conditions. The water flux in the H90 module was 1.41 LMH, while the flux in the H180 module was 1.17 LMH. As described in section 2.3.1, the initial linear velocity on the bore side was higher for the H90 module than for the H180 module because the number of HFs in the H90 module is half that in the H180 module. This means that the dilution rate caused by water permeation is expected to be lower for the H90 module than the H180 module because the retention period of solution in the bore becomes shorter as the flow rate increases. The concentration difference between the bore side and the shell side is consequently lower in the H90 module than in the H180 module, which means that the osmotic pressure difference, $\Delta\pi_{eff}$, in the H90 module is smaller than that in H180 module. This results in the effective applied pressure ($\Delta P - \Delta\pi_{eff}$) being higher in the H90 module than in the H180 module. The water flux in the H90 module was therefore higher than that in the H180 module.

The H180 module concentrated the shell-side feed solution by a factor of 1.042 after three hours operation, while the H90 feed was concentrated 1.022 times. This result is attributed to the difference in total membrane area. The total membrane area of the H180 module is 2.80×10^{-2} m^2, while that of the H90 module is 1.40×10^{-2} m^2 (Table 1). The total permeated water after three hours' operation was 9.83×10^{-2} L (= 1.17 L m^{-2} h^{-1} × 2.80×10^{-2} m^2 × 3 h) for the H180 module and 5.92×10^{-2} L (= 1.41 L m^{-2} h^{-1} × 1.40×10^{-2} m^2 × 3 h) for the H90 module. The feed solution volume was 2.5 L, as described in Section 2.3.1. After three hours' operation, the concentration ratio between the H180 and H90 modules is given by $(2.5 - 5.92\times10^{-2}) / (2.5 - 9.83\times10^{-2}) = 1.02$. This value is consistent with the comparison value: 1.042/1.022=1.02.

It is clear from the preceding discussion that the degree of concentration of the H180 module is higher than that of the H90 module since the volume of total permeated water was larger for the H180 module than for the H90 module even though the water flux of H180 module is lower than that of the H90 module. The H180 module was therefore chosen for the subsequent multistage concentration tests.

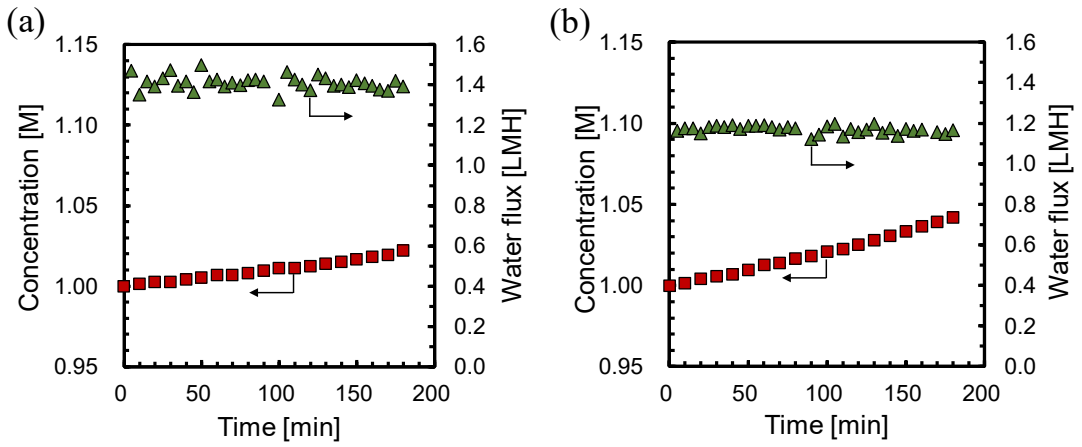

Fig. 8 Single-stage concentration test, (a) H90 module and (b) H180 module.

3.2.2 Multistage concentration test

A ten-stage concentration test was performed to evaluate the multistage concentration performance. The operation time in each stage was 180 minutes, which was same as that in the single-stage operation shown in Fig. 8. Figure 9 shows the concentration of concentrated solution and the water flux at each stage. As shown in Fig. 9(a), the concentration was increased from 1.0 M to 1.12 M at an initial feed solution concentration C_0 = 1.0 M and ΔP = 15 bar, while the concentration was increased from 1.0 M to 1.042 M in single-stage operation (Fig. 8(b)) under the same conditions. This clearly demonstrates that the degree of concentration is enhanced as expected by multistage operation.

A comparison of Figs. 9(a) and (b) shows that the water flux decreases with increasing initial feed concentration. This is because the ICP shown in Fig.2 increases with the feed concentration, resulting in a decrease in the effective applied pressure driving force. Figure 10 shows the osmotic pressure

caused by ICP, $\Delta\pi_{ICP}$, and the apparent water permeability as a function of feed concentration at an applied pressure of 15 bar whose $\Delta\pi_{ICP}$ and apparent water permeability were calculated from a permeability model in OARO shown in our previous work (Togo et al., 2019). The concentration ratio after the 10th stage in Fig. 9(b) is about 1.06 (= 2.12 / 2), while that in Fig. 9(a) is about 1.12 (= 1.12 / 1). The final concentration ratio for higher initial feed concentration is lower than that for lower initial feed concentration because the water flux is lower.

Figures 9(a) and (c) show that solution concentration increases with higher applied pressure. This is due to the higher water flux caused by the increase in the effective applied pressure. Similar results were obtained in the case using a pilot-scale HF membrane module in the pressure range from 8 to 12 bar (Togo et al., 2019). Lower initial feed concentration and higher applied pressure result in a higher degree of concentration. However, it is also clear from Figs. 9 and 10 that the osmotic pressure increases with the feed concentration because of the increase in ICP, which results in a decrease in the effective applied pressure under the same externally applied pressure. This limits the degree of concentration achievable by OARO processes, and the limit depends on the feed concentration and applied pressure. The concentration process stops when the osmotic pressure due to ICP becomes equal to the externally applied pressure. In regard to ICP, the membrane with less affected ICP (low S parameter) would be suitable for the achievement of high concentration by OARO process.

There is a potential for higher solution concentration up to the solubility of NaCl around 5 M. For the OARO process using NaCl aqueous solution with high concentration, some factors would affect the solution concentration. The viscosity increases with the solution concentration (Goldsack and Franchetto, 1978), and the increase of the viscosity of the NaCl solution decrease the diffusion rate, which results in the increase in ICP (McCutcheon and Elimelech, 2006). In addition, an electrical interaction between membrane and charged ions is screened in high concentration solution, which leads to the decrease of the electrostatic repulsion and rejection performance (Nghiem et al., 2006). Thus, an evaluation of the membrane performance in various concentration condition is important, especially for high concentration solution. At the same time, much attention needs to be paid to a purity of the solution for such a high concentration process to prevent the risk of a membrane scaling and concentration of impurities.

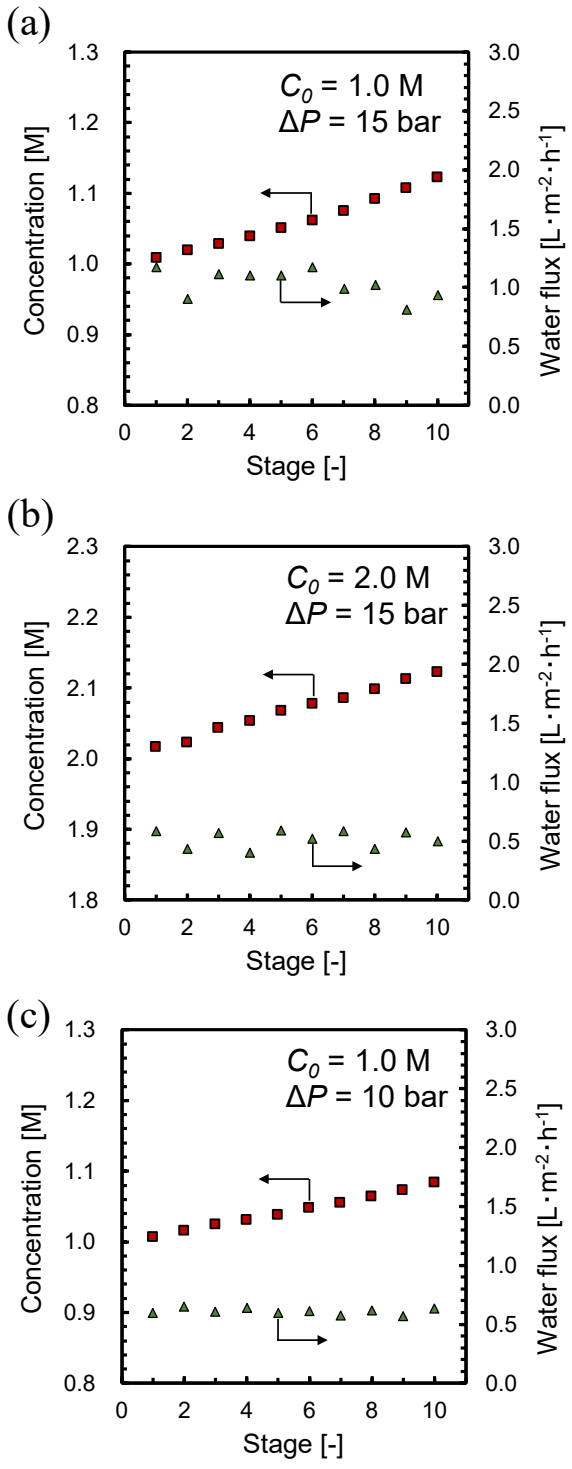

Fig. 9 Multistage concentration test with H180 module. (a): C_0=1.0 M NaCl, ΔP=15 bar, (b): C_0=2.0 M NaCl, ΔP=15 bar, (c): C_0=1.0 M NaCl, ΔP=10 bar. C_0 indicates the initial feed solution concentration, and ΔP, the applied pressure.

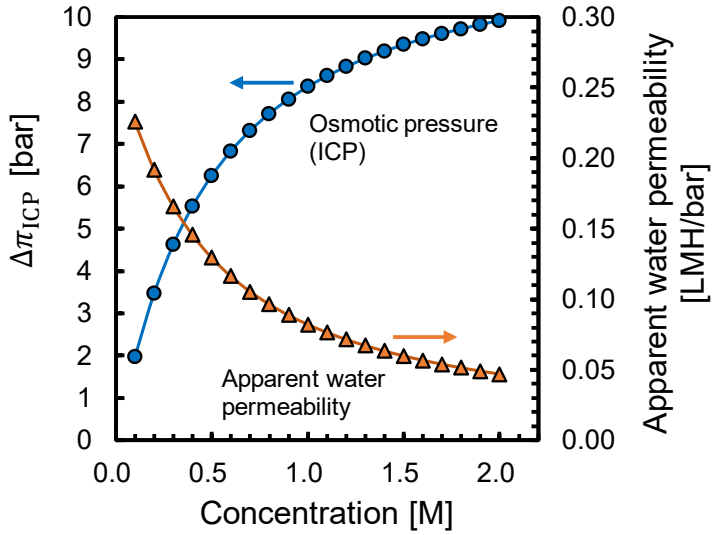

Fig. 10 Internal concentration polarization, $\Delta\pi_{ICP}$, and apparent water permeability as a function of feed concentration; Figure reproduced from Togo et al. (Togo et al., 2019).

The OARO performances for the multistage concentration process using H180 module were compared with the previous results which were obtained in the single-stage concentration process using a pilot-scale HF membrane module (Togo et al., 2019) in the similar experimental condition (membrane: CTA HF, solution: 1.0 M NaCl, ΔP: 10 bar, linear velocity: around 0.01 m/s), although the module structure was different. The multistage concentration using H180 module showed higher water flux (0.6 LMH) than the single concentration process using a pilot-scale HF membrane module (0.4 LMH). On the other hand, the concentration after the 10th stage using H180 module (1.08 M) was nearly equal to that for the single-stage concentration process using a pilot-scale HF membrane module (1.09 M). Considering from the module lengths (0.245 m for H180 module and 0.58 m for pilot-scale module), the effective concentration was achieved for the pilot-scale HF membrane module because

of the difference of module structure and effective membrane area. Thus, the concentration can be enhanced by multistage operation, and the structure of membrane module also plays an important role in the effective concentration. Further improvement such as a utilization of recycle systems of the diluted permeation is necessary to enhance the recovery rate in the multistage OARO process in the near future.

4. Conclusions

We tested the concentration of NaCl solution by a multistage OARO system with two types of CTA HF membrane modules. Water permeated through the membrane, and the feed solution was concentrated by the OARO process even using highly concentrated NaCl solutions (1.0 and 2.0 M) and low applied pressures (10 and 15 bar). A multistage system produced a higher degree of concentration as compared with a single stage system. When the initial feed concentration was high, the water flux and concentration ratio were lower as compared with low initial feed concentration. This is due to the effect of ICP. Therefore, increasing the applied pressure and optimizing membrane performance are advisable to maintain a high degree of concentration in the latter stages of a multistage OARO system.

Owing to the advantages of lower operating temperature and lower energy consumption as compared with conventional methods, the OARO process is expected to be applied in the concentration processes in the food industry such as juice. It is thus believed that OARO process may have great potential for various practical applications.

Conflicts of interest

The authors have no conflicts of interest to declare.

Table captions

Table 1 Specifications of HF membrane modules

Figure captions

Fig. 1 Concept of osmotically assisted reverse osmosis (OARO).

Fig. 2 Concentration polarization under OARO operation. ECP: external concentration polarization, ICP: internal concentration polarization, $\Delta\pi_{eff}$: effective osmotic pressure difference at interface.

Fig. 3 Schematic of HF membrane module.

Fig. 4 Schematic of module evaluation system.

Fig. 5 Schematic of single stage concentration process.

Fig. 6 Schematic of 2 connected stages in a multistage OARO process.

Fig. 7 Water flux (a, b), salt permeability coefficient (c), and salt rejection (d) of H90 (a, c) and H180 module (b, d) as a function of applied pressure.

Fig. 8 Single stage concentration test: (a) H90 module and (b) H180 module.

Fig. 9 Multistage concentration test with H180 module. (a): C_0=1.0 M NaCl, ΔP=15 bar, (b): C_0=2.0 M NaCl, ΔP=15 bar, (c): C_0=1.0 M NaCl, ΔP=10 bar. C_0 indicates the initial feed solution concentration and ΔP, the applied pressure.

Fig. 10 Internal concentration polarization, $\Delta\pi_{CP}$, and the apparent water permeability as a function of feed concentration; reproduced from Togo et al.(Togo et al., 2019).

References

Alvarez, V., Alvarez, S., Riera, F.A., Alvarez, R., 1997. Permeate flux prediction in apple juice concentration by reverse osmosis. J. Membr. Sci. 127, 25–34. https://doi.org/10.1016/S0376-7388(96)00285-2

Bartholomew, T. V., Mey, L., Arena, J.T., Siefert, N.S., Mauter, M.S., 2017. Osmotically assisted reverse osmosis for high salinity brine treatment. Desalination 421, 3–11. https://doi.org/10.1016/j.desal.2017.04.012

Bartholomew, T. V., Siefert, N.S., Mauter, M.S., 2018. Cost Optimization of Osmotically Assisted Reverse Osmosis. Environ. Sci. Technol. 52, acs.est.8b02771. https://doi.org/10.1021/acs.est.8b02771

Chekli, L., Phuntsho, S., Kim, J.E., Kim, J., Choi, J.Y., Choi, J.-S., Kim, S., Kim, J.H., Hong, S., Sohn, J., Shon, H.K., 2016. A comprehensive review of hybrid forward osmosis systems: Performance, applications and future prospects. J. Membr. Sci. 497, 430–449. https://doi.org/10.1016/j.memsci.2015.09.041

Chen, X., Yip, N.Y., 2018. Unlocking High-Salinity Desalination with Cascading Osmotically Mediated Reverse Osmosis: Energy and Operating Pressure Analysis. Environ. Sci. Technol. 52, 2242–2250. https://doi.org/10.1021/acs.est.7b05774

Ge, Q., Ling, M., Chung, T.S., 2013. Draw solutions for forward osmosis processes: Developments, challenges, and prospects for the future. J. Membr. Sci. 442, 225–237. https://doi.org/10.1016/j.memsci.2013.03.046

Goldsack, D.E., Franchetto, R.C., 1978. The viscosity of concentrated electrolyte solutions. II. Temperature dependence. Can. J. Chem. 56, 1442–1450. https://doi.org/10.1139/v78-236

Jesus, D.F., Leite, M.F., Silva, L.F.M., Modesta, R.D., Matta, V.M., Cabral, L.M.C., 2007. Orange (Citrus sinensis) juice concentration by reverse osmosis. J. Food Eng. 81, 287–291. https://doi.org/10.1016/j.jfoodeng.2006.06.014

Jiao, B., Cassano, A., Drioli, E., 2004. Recent advances on membrane processes for the concentration of fruit juices: a review. J. Food Eng. 63, 303–324. https://doi.org/10.1016/j.jfoodeng.2003.08.003

Kim, J., Kim, D.I., Hong, S., 2018a. Analysis of an osmotically-enhanced dewatering process for the treatment of highly saline (waste)waters. J. Membr. Sci. 548, 685–693. https://doi.org/10.1016/j.memsci.2017.10.048

Kim, Jungwon, Kim, Jungbin, Kim, Junghyun, Hong, S., 2018b. Osmotically enhanced dewatering-reverse osmosis (OED-RO) hybrid system: Implications for shale gas produced water treatment. J. Membr. Sci. 554, 282–290. https://doi.org/10.1016/j.memsci.2018.03.015

McCutcheon, J.R., Elimelech, M., 2006. Influence of concentrative and dilutive internal concentration polarization on flux behavior in forward osmosis. J. Membr. Sci. 284, 237–247. https://doi.org/10.1016/j.memsci.2006.07.049

Nghiem, L.D., Schäfer, A.I., Elimelech, M., 2006. Role of electrostatic interactions in the retention of pharmaceutically active contaminants by a loose nanofiltration membrane. J. Membr. Sci. 286, 52–59. https://doi.org/10.1016/j.memsci.2006.09.011

Park, K., Kim, D.Y., Yang, D.R., 2017. Cost-based feasibility study and sensitivity analysis of a new draw solution assisted reverse osmosis (DSARO) process for seawater desalination. Desalination 422, 182–193. https://doi.org/10.1016/j.desal.2017.08.026

Petrotos, K.B., Lazarides, H.N., 2001. Osmotic concentration of liquid foods. J. Food Eng. 49, 201–206. https://doi.org/10.1016/S0260-8774(00)00222-3

Sant'Anna, V., Marczak, L.D.F., Tessaro, I.C., 2012. Membrane concentration of liquid foods by forward osmosis: Process and quality view. J. Food Eng. 111, 483–489. https://doi.org/10.1016/j.jfoodeng.2012.01.032

Shibuya, M., Sasaki, K., Tanaka, Y., Yasukawa, M., Takahashi, T., Kondo, A., Matsuyama, H., 2017. Development of combined nanofiltration and forward osmosis process for production of ethanol from pretreated rice straw. Bioresour. Technol. 235, 405–410. https://doi.org/10.1016/j.biortech.2017.03.158

Sukitpaneenit, P., Chung, T.S., 2012. High performance thin-film composite forward osmosis hollow fiber membranes with macrovoid-free and highly porous structure for sustainable water production. Environ. Sci. Technol. 46, 7358–7365. https://doi.org/10.1021/es301559z

Togo, N., Nakagawa, K., Shintani, T., Yoshioka, T., Takahashi, T., Kamio, E., Matsuyama, H., 2019. Osmotically Assisted Reverse Osmosis Utilizing Hollow Fiber Membrane Module for Concentration Process. Ind. Eng. Chem. Res. 58, 6721–6729. https://doi.org/10.1021/acs.iecr.9b00630

Yasukawa, M., Mishima, S., Shibuya, M., Saeki, D., Takahashi, T., Miyoshi, T., Matsuyama, H., 2015. Preparation of a forward osmosis membrane using a highly porous polyketone

microfiltration membrane as a novel support. J. Membr. Sci. 487, 51–59. https://doi.org/10.1016/j.memsci.2015.03.043

Zhang, S., Wang, K.Y., Chung, T.S., Chen, H., Jean, Y.C., Amy, G., 2010. Well-constructed cellulose acetate membranes for forward osmosis: Minimized internal concentration polarization with an ultra-thin selective layer. J. Membr. Sci. 360, 522–535. https://doi.org/10.1016/j.memsci.2010.05.056

Zhang, Y., Nakagawa, K., Shibuya, M., Sasaki, K., Takahashi, T., Shintani, T., Yoshioka, T., Kamio, E., Kondo, A., Matsuyama, H., 2018. Improved permselectivity of forward osmosis membranes for efficient concentration of pretreated rice straw and bioethanol production. J. Membr. Sci. 566, 15–24. https://doi.org/10.1016/j.memsci.2018.08.046